# A Radar Backscatter Model for Discontinuous Coniferous Forests

Guoqing Sun, David S. Simonett, and Alan H. Strahler, *Member, IEEE*

***Abstract*—A radar backscattering model for low to medium density woodland is described in this paper, in which each tree is treated as an individual backscatterer. A forest stand viewed by radar is then an assemblage of scatterers standing on a background in a certain spatial pattern. The backscattering components arising from the various intersections of radar beams with the forest stand are calculated separately and their Stokes matrices are then added together to achieve the Stokes matrix for total backscattering. Probabilities of radar beams intersecting tree crowns are introduced into the model in calculating the backscattering and to give each component the appropriate extinctions.**

***Keywords*—Discontinuous forest canopies, Stokes matrix, gap probabilities.**

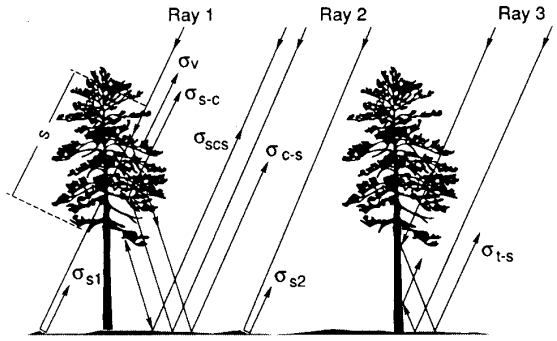


Fig. 1. Backscattering components of a discontinuous forest canopy.

## I. Introduction

A number of microwave backscattering models of forests have been developed over the past several years [1]–[6], in which the forest stands are treated as continuous layers in the horizontal direction. The specific forest parameters have been directly used as model inputs and the backscattering characteristics of various forest stands have been reasonably predicted from these models. For modeling forest stands of low-to-medium densities, this paper presents a radar backscattering model for discontinuous forest stands in which each tree is treated as an individual backscatter. A forest stand viewed by radar is then an assemblage of scatterers standing on a background in a certain spatial pattern. The shape, size, and position distribution are determined by the forest structure in a given successional stage. The major driving parameters of this model are the most important physical parameters of a forest; i.e., tree number per unit area and average tree heights in a stand.

The major scattering mechanisms considered in this model are the same as in the *L*-band *HH* backscatter model developed by Richards *et al.* [1]. The current model, however, will predict backscattering Stokes matrix from a forest stand. The radar beam may be considered to be of three different types in terms of its intersection with forest stands: 1) Intersecting at least one tree crown; 2) intersecting no tree—i.e., incident directly on the soil surface through gaps between trees and producing a direct surface backscattering; and 3) encountering a tree trunk and giving a strong specular scattering involving trunk-ground interaction, especially if the surface is relatively smooth. The backscattering components associated with beam 1 include (see Fig. 1): (a) Volume backscattering from the tree crown, $\sigma_v$ (leaves and branches); (b) direct backscattering from the surface area shadowed by tree crown $\sigma_{s1}$; and (c) an interaction component between tree crown and ground surface $\sigma_{t-s}$, which includes three terms; ground-crown ($\sigma_{s-c}$), crown-ground ($\sigma_{c-s}$), and ground-crown-ground ($\sigma_{scs}$) terms. Backscattering components for beam 2 are $\sigma_{s2}$, and for beam 3 include $\sigma_{t-s}$. These components are considered to be phase-independent so that the Stokes matrices of these components may be added together to obtain the Stokes matrix for the total backscattering of the forest stand. Probabilities of radar beams intersecting tree crowns are introduced into the model in calculating the backscattering and to give each component the appropriate extinctions. Multiple scattering between cylinders is not considered in the present model.

The tree crown is modeled as a homogeneous ellipsoid comprised of scattering elements (needles and cylinders for coniferous trees) with various size and orientations. The scattering and extinction properties of an arbitrarily

Manuscript received July 27, 1990; revised March 15, 1991. This work was supported by NASA Contracts through the Jet Propulsion Laboratory as part of SIR-B and SIR-C Science Investigations.

Q. Sun is with Resseler Associates, Inc., Laurel, MA 20707.

D. S. Simonett was with the Department of Geography, University of California, Santa Barbara, Santa Barbara, CA. He passed away in December 1990.

A. H. Strahler is with the Department of Geography, Boston University, Boston, MA 02215.

IEEE Log Number 9100472.

0196-2892/91/0700-0639$01.00 © 1991 IEEE

oriented dielectric cylinder are calculated and then integrated over its size and orientation distributions (Section II). Multiplying by the number of cylinders per unit volume, the averaged properties were used as parameters in the radiative transfer equation to calculate the components associated with the crown. Section III gives the formulae for the four major backscattering components in the model. The trunks are assumed either to be vertical to the ground or to have a specified orientation distribution. The backscattering of ground surface was calculated by use of an appropriate surface-scattering model based on the surface roughness and radar wavelength. The extinction suffered by each component is dependent on the probabilities of the radar beam intersecting none, one, two, $\cdots$, $n$ trees. For low density stands (2–15 trees per $25 \times 25$ m$^2$ pixel), the probabilities of intersecting more than two trees are very small. Section IV describes various extinctions suffered by each backscattering component.

Model sensitivity analysis and simulation results are presented in Sections V and VI, along with the discussions on various issues involving model inputs and simulation results.

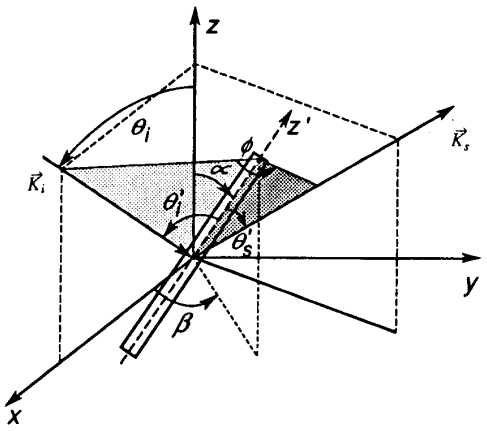


Fig. 2. Scattering geometry of a dielectric cylinder.

where $(\boldsymbol{E}_v^i, \boldsymbol{E}_h^i)$ and $(\boldsymbol{E}_v^s, \boldsymbol{E}_h^s)$ are the incident and scattering fields. The Stokes matrix $\boldsymbol{L}$, which describes the relation between incidence and scattered Stokes vectors, may be derived from the complex scattering matrix by [3], [9], [10]:

$$\boldsymbol{L} = \begin{bmatrix} \boldsymbol{S}_{vv}\boldsymbol{S}_{vv}^* & \boldsymbol{S}_{vh}\boldsymbol{S}_{vh}^* & \text{Re}\,(\boldsymbol{S}_{vh}\boldsymbol{S}_{vv}^*) & -\text{Im}\,(\boldsymbol{S}_{vh}^*\boldsymbol{S}_{vv}) \\ \boldsymbol{S}_{hv}\boldsymbol{S}_{hv}^* & \boldsymbol{S}_{hh}\boldsymbol{S}_{hh}^* & \text{Re}\,(\boldsymbol{S}_{hh}^*\boldsymbol{S}_{hv}) & -\text{Im}\,(\boldsymbol{S}_{hh}^*\boldsymbol{S}_{hv}) \\ 2\,\text{Re}\,(\boldsymbol{S}_{vv}\boldsymbol{S}_{hv}^*) & 2\,\text{Re}\,(\boldsymbol{S}_{vh}\boldsymbol{S}_{hh}^*) & \text{Re}\,(\boldsymbol{S}_{vv}\boldsymbol{S}_{hh}^* + \boldsymbol{S}_{vh}\boldsymbol{S}_{hv}^*) & -\text{Im}\,(\boldsymbol{S}_{vv}\boldsymbol{S}_{hh}^* - \boldsymbol{S}_{vh}\boldsymbol{S}_{hv}^*) \\ 2\,\text{Im}\,(\boldsymbol{S}_{vv}\boldsymbol{S}_{hv}^*) & 2\,\text{Im}\,(\boldsymbol{S}_{vh}\boldsymbol{S}_{hh}^*) & \text{Im}\,(\boldsymbol{S}_{vv}\boldsymbol{S}_{hh}^* + \boldsymbol{S}_{vh}\boldsymbol{S}_{hv}^*) & \text{Re}\,(\boldsymbol{S}_{vv}\boldsymbol{S}_{hh}^* - \boldsymbol{S}_{vh}\boldsymbol{S}_{hv}^*) \end{bmatrix}. \tag{2}$$

## II. Scattering and Extinction from Tree Crown

Fig. 2 depicts the scattering geometry of a finite-length circular cylinder. The orientation of the cylinder is determined by zenith angle $\alpha$ and azimuth angle $\beta$. The incidence wave is in the plane $XOZ$ and forms an angle $\theta_i$ with the $Z$-axis. The $XYZ$ coordinate system is referred to as the primary system, from which the orientations of cylinder, incidence, and scattering directions are defined.

The scattering matrix of a vertically oriented cylinder with finite length can be calculated using the equations given by Ruck *et al.* [7] and Bohren and Huffman [8]. For an arbitrarily oriented dielectric cylinder, the incidence plane is now made by the incident wave vector $\vec{k}_i$ and cylinder orientation vector $\vec{z}'$, and the scattering plane is the plane made by vector $\vec{z}$ and scattering wave vector $\vec{k}_s$. The $\vec{x}$ of the local coordinate system is in the incident plane. We can determine the scattering matrix of the cylinder within the local coordinate system $X'Y'Z'$ and then transform it to the primary system $XYZ$.

The scattering from a scatterer can be characterized by the complex scattering matrix $\boldsymbol{S}_{pq}$, defined according to:

$$\begin{bmatrix} \boldsymbol{E}_v^s \\ \boldsymbol{E}_h^s \end{bmatrix} = \frac{e^{ikr}}{r} \begin{bmatrix} \boldsymbol{S}_{vv} & \boldsymbol{S}_{vh} \\ \boldsymbol{S}_{hv} & \boldsymbol{S}_{hh} \end{bmatrix} \begin{bmatrix} \boldsymbol{E}_v^i \\ \boldsymbol{E}_h^i \end{bmatrix} \tag{1}$$

In order to model the scattering from a volume of dielectric cylinders with a specified orientation distribution, the scattering function or Stokes matrix needs to be averaged over all orientations $(\alpha, \beta)$ and sizes $(h, a)$ of the cylinders.

If the scatterings from the cylinders have independent phases, the Stokes matrices can be integrated to achieve the scattering of an averaged effective cylinder:

$$\langle \boldsymbol{P}(\theta_i, \theta_s, \phi)\rangle = \int_{\alpha_1}^{\alpha_2} d\alpha \int_{\beta_1}^{\beta_2} d\beta \int_{h_1}^{h_2} dh \int_{a_1}^{a_2} da \cdot \boldsymbol{L}(\alpha, \beta; h, a, \theta_i, \theta_s, \phi) p_1(\alpha, \beta) p_2(h, a) \tag{3}$$

where $p_1$ and $p_2$ are the probability distributions of cylinder orientation and size, respectively.

The total power loss from the incident wave due to the scattering and absorption of a wave by the scatterer is closely related to the behavior of the scattered field in the forward direction. For a medium with low concentration of scatterers and by applying the optical theorem, the total extinction cross section can be calculated when the scattering amplitude in the forward direction is known [10]. The extinction coefficient matrix $\kappa$ below is used to de-

scribe the volume extinction property of tree foliage:

$$\kappa = -\begin{bmatrix} 2\,\mathrm{Re}\,(M_{vv}) & 0 & \mathrm{Re}\,(M_{vh}) & \mathrm{Im}\,(M_{vh}) \\ 0 & 2\,\mathrm{Re}\,(M_{hh}) & \mathrm{Re}\,(M_{hv}) & -\mathrm{Im}\,(M_{hv}) \\ 2\,\mathrm{Re}\,(M_{hv}) & 2\,\mathrm{Re}\,(M_{vh}) & \mathrm{Re}\,(M_{vv}+M_{hh}) & \mathrm{Im}\,(M_{hh}-M_{vv}) \\ -2\,\mathrm{Im}\,(M_{hv}) & 2\,\mathrm{Im}\,(M_{vh}) & \mathrm{Im}\,(M_{vv}-M_{hh}) & \mathrm{Re}\,(M_{hh}+M_{vv}) \end{bmatrix} \tag{4}$$

and

$$M_{pq} = \frac{2\pi i N}{k} \langle S_{pq}(\theta, \pi - \theta, \pi)\rangle \tag{5}$$

where the $p$, $q$ stand for polarizations $h$ or $v$, $\langle S_{pq}(\theta, \pi - \theta, \pi)\rangle$ is the averaging of forward scattering matrix by an integration similar to (3). The $N$ is the number of scattering elements per cubic meter and $k$ wavenumber.

The Stokes and extinction matrix of needles were calculated using equations provided in [3] and [10]. The sum of the Stokes and extinction matrices for needles and branches were used as the volume properties of tree crown for calculating the backscattering components in the next two sections.

## III. Four Major Backscattering Components

Fig. 1 shows the backscattering components considered in the current model. In addition to the direct backscattering from tree crown and ground surface, the interaction component between tree crown and ground surface consists of three terms, as mentioned before, and the trunk–surface double bounce component consists of two terms in opposite directions.

The scattering and extinction are dependent on the pathlength $s$ of radar beams within the tree crown. For an ellipsoidal crown with two radii $H$ and $R$ ($w = H/R$), the probability density function of $s$ at incidence angle $\theta$ is [11]:

$$P(s) = \frac{s}{2(RG)^2} \tag{6}$$

with $s$ ranging from 0 to $2RG$ and $G = [(1 + w^2 \tan^2\theta)/(1 + \tan^2\theta)]^{1/2}$. Therefore the scattering terms $\boldsymbol{M}_*(s)$ (the * can be $v$, $scs$, $c - s$, $s - c$) to be calculated below should be averaged by the following integration:

$$\boldsymbol{M}_*^0 = \int_0^{s_0} P(s)\boldsymbol{M}_*(s)\, ds, \qquad s_0 = 2RG. \tag{7}$$

### A. Volume Backscattering from Tree Crowns

Obviously, calculating backscattering from tree crown by solving the radiative transfer equation is not an easy task, because of the complex boundary conditions. For approximation, results from the solution of the radiative transfer equation for layered media [3] were adopted here. When a ray passes a tree crown (see Ray 1 in Fig. 1), a horizontal layer from the entrance point to the exit point was assumed. For a layer of canopy with depth $s\mu_0$ at the incidence $(-\mu_0, \phi_0)$, with $\mu_0 = \cos(\theta_i)$, the first-order solution for canopy volume backscattering at direction $(\mu, \phi)$ is

$$\boldsymbol{M}_v = \boldsymbol{Q}_c(\mu, \phi)\boldsymbol{A}_4\boldsymbol{Q}_c^{-1}(-\mu_0, \phi_0) \tag{8}$$

where [3, equation (A.39)]

$$\boldsymbol{A}_4 = \int_{-s\mu_0}^{0} \boldsymbol{D}_c(\mu, \phi; z/\mu)\boldsymbol{Q}_c^{-1}(\mu, \phi)\boldsymbol{P}_c(\mu, \phi; -\mu_0, \phi_0) \cdot \boldsymbol{Q}_c(-\mu_0, \phi_0)\boldsymbol{D}_c(-\mu_0, \phi_0; z/\mu_0)\, dz \tag{9}$$

whose $(i, j)_{\text{th}}$ element is given by

$$[\boldsymbol{A}_4]_{ij} = \frac{1 - \exp[-(\Lambda_i(\mu, \phi)/\mu + \Lambda_j(-\mu_0, \phi_0)/\mu_0)s\mu_0]}{\Lambda_i(\mu, \phi)/\mu + \Lambda_j(-\mu_0, \phi_0)/\mu_0} \cdot [\boldsymbol{Q}_c^{-1}(\mu, \phi)\boldsymbol{P}_c(\mu, \phi; -\mu_0, \phi_0)\boldsymbol{Q}_c(-\mu_0, \phi_0)]_{ij} \tag{10}$$

where $\boldsymbol{P}_c$ is the averaged Stokes matrix in the backscattering direction described in Section II. The $\Lambda_i$ and $\Lambda_j$, with $i, j = 1, 2, 3, 4$, are the eigenvalues of extinction matrix of tree crown, $\boldsymbol{Q}_c$ is the corresponding matrix of eigenvectors, and $\boldsymbol{D}_c$ is a diagonal matrix accounting for the extinction of tree crown [3], [10].

The probability of path length ($s$) of radar ray through a tree crown can be expressed by (6), and $\boldsymbol{A}_4$ should be averaged over the crown by the integration mentioned above. By implementing the integration and noting that $\mu = \mu_0$, we obtain

$$[\bar{\boldsymbol{A}}_4]_{ij} = \mu_0 [\boldsymbol{G}_1]_{ij} \cdot [\boldsymbol{Q}_c^{-1}(\mu, \phi)\boldsymbol{P}_c(\mu, \phi; -\mu_0, \phi_0) \cdot \boldsymbol{Q}_c(-\mu_0, \phi_0)]_{ij} \tag{11}$$

and

$$[\boldsymbol{G}_1]_{ij} = \frac{1}{\Lambda} + \left(\frac{2}{\Lambda^2 s_0} + \frac{2}{\Lambda^3 s_0^2}\right)\exp(-\Lambda s_0) - \frac{2}{\Lambda^3 s_0^2}$$

$$\Lambda = \Lambda_i(\mu, \phi) + \Lambda_j(-\mu_0, \phi_0)$$

where $s_0$ is the upper limit of pathlength $s$; i.e., $2RG$.

### B. Ground–Crown Interaction Term

The three components associated with the canopy–ground interaction are given below.

*Radar–Ground–Crown–Ground–Radar Term:*

$$\boldsymbol{M}_{scs} = \boldsymbol{P}_s \boldsymbol{Q}_c(-\mu, \phi)\boldsymbol{A}_1 \boldsymbol{Q}_c^{-1}(\mu_0, \phi_0)\boldsymbol{P}_s. \quad (12)$$

*Radar–Crown–Ground–Radar Term:*

$$\boldsymbol{M}_{c-s} = \boldsymbol{P}_s \boldsymbol{Q}_c(-\mu, \phi)\boldsymbol{A}_2 \boldsymbol{Q}_c^{-1}(-\mu_0, \phi_0). \quad (13)$$

*Radar–Ground–Crown–Radar Term:*

$$\boldsymbol{M}_{s-c} = \boldsymbol{Q}_c(\mu, \phi)\boldsymbol{A}_3 \boldsymbol{Q}_c^{-1}(\mu_0, \phi_0)\boldsymbol{P}_s \quad (14)$$

with the $\boldsymbol{A}_1$ has a similar form with $\boldsymbol{A}_4$, because both are related to the backscattering from the canopy, and after integrations, $\boldsymbol{A}_2$ and $\boldsymbol{A}_3$ have similar forms as follows:

$$[\bar{\boldsymbol{A}}_2]_{ij} = [\boldsymbol{G}_2]_{ij} \cdot [\boldsymbol{Q}_c^{-1}(\mu, \phi)\boldsymbol{P}_c(\mu, \phi; -\mu_0, \phi_0) \cdot \boldsymbol{Q}_c(-\mu_0, \phi_0)]_{ij} \quad (15)$$

where

$$[\boldsymbol{G}_2]_{ii} = \frac{4\mu_0}{\Lambda_i^3 s_0^2} - \left(\frac{2}{\Lambda_i} + \frac{4}{\Lambda_i^2 s_0} + \frac{4}{\Lambda_i^3 s_0^2}\right)\mu_0 \exp(-\Lambda_i s_0), \quad \text{if } i = j$$

and

$$[\boldsymbol{G}_2]_{ij} = \frac{2}{(\Lambda s_0^2)}\left(\frac{1}{\Lambda_2^2} - \frac{1}{\Lambda_1^2} - \frac{1}{\Lambda_2} e^{-\Lambda_2 s_0}\left(s_0 + \frac{1}{\Lambda_2}\right) + \frac{1}{\Lambda_1} e^{-\Lambda_1 s_0}\left(s_0 + \frac{1}{\Lambda_1}\right)\right)$$

if $i \neq j$, where $\Lambda = \Lambda_1 - \Lambda_2$, $\Lambda_1 = \Lambda_i(\mu, \phi)$, and $\Lambda_2 = \Lambda_j(\mu_0, \phi_0)$. $\boldsymbol{P}_s$ is the Stokes matrix of the ground surface at the specular direction. Because most of the surface in our study area (South-east forests of Mount Shasta, northern California) is very smooth, $\boldsymbol{P}_s$ was calculated by

$$\boldsymbol{P}_s = \rho \exp[-2(k\sigma \cos\theta_i)^2] \quad (16)$$

where $\rho$ is the Fresnel reflectance matrix of the surface, $\sigma$ here is the standard deviation of surface height, and $k$ is the wave number.

### C. Backscattering from the Ground Surface

The direct backscattering Stokes matrix of the ground surface $\boldsymbol{M}_s(-\mu_0, \phi_0; \mu_0, \phi_0)$ can be calculated by use of an appropriate surface-scattering model based on surface roughness and radar wavelength. A small perturbation model was used in this study, since the surface is quite smooth.

### D. Ground–Trunk Interaction Term

The trunks are treated as dielectric cylinders in this model as before [5]. Because the number of trees per pixel is assumed to be low for discontinuous forest stands, the only attenuation considered arising from the trunks is the shadows on the direct surface backscattering.

The scattering matrix for each tree in a pixel was converted to the Stokes matrix and then summed to get the total scattering from trunks [12]. The term $\boldsymbol{M}_{t-s}$ is calculated by

$$\boldsymbol{M}_{t-s} = \sum_{i=0}^{i=n} [\boldsymbol{P}_t^i(\mu_0, \phi_0; \mu, \phi) \cdot \boldsymbol{P}_s(-\mu_0; \mu) + \boldsymbol{P}_s(-\mu_0, \mu) \cdot \boldsymbol{P}_t^i(-\mu_0, \phi_0; -\mu, \phi) + \boldsymbol{P}_t^i(-\mu_0, \phi_0; -\mu, \phi)]/PA \quad (17)$$

where the first two terms represent scatterings in opposite directions, and the third term is the direct backscattering from the trunk, which may be significant if the trunk is not vertical to the ground surface and nearly perpendicular to the incidence waves. The $PA$ stands for the total surface area of a pixel, and $n$ is the total number of trunks in the pixel.

The four major backscattering components calculated above will suffer attenuations if there were tree crowns between the scatterers and radar. These extinctions are dependent on the probability of radar-wave-passing tree crowns and are discussed in the next section.

## IV. Calculations of Backscattering Coefficient

The probability that a radar beam intersects $n$ tree crowns is $P(n) = \mu^n e^{-\mu}/n!$ (Fig. 3) [13], where $\mu = cA$, $c$ is the average tree count per unit area, and $A$ is the average projected shadow area of a tree crown on the ground. The sum of the probabilities is

$$\sum_{n=0}^{n=\infty} P(n) = 1.$$

Here the distribution of tree size is assumed to be log-normal and trees are randomly positioned within a stand (Poisson distribution).

Appropriate attenuation terms have to be introduced into the backscattering coefficients calculated in the above section. By combining gap probabilities and the extinction matrix and the average path-length of the radar beam within a tree crown ($\bar{s}$), the final forms for the model components are as follows: The $P(n)$ used in the following equations represents the probability of a radar ray passing through $n$ tree crowns. The factor $e^{-\kappa_c \bar{ns}}$ is the extinction by a tree crown when the wave is passing through it downwardly, while $e^{-\kappa_c^+ \bar{ns}}$ means upward extinction (see [3, equation A.16]).

### A. Volume Backscattering from Tree Crowns

$$\boldsymbol{M}_v^0 = \sum_{n=1}^{n=\infty} [P(n) e^{-\kappa_c^+ (n-1)\bar{s}}) \boldsymbol{M}_v e^{-\kappa_c (n-1)\bar{s}}]. \quad (18)$$

The first term in this equation (when $n = 1$) is $P(1)\boldsymbol{M}_v$, which is the direct backscattering from some tree crowns

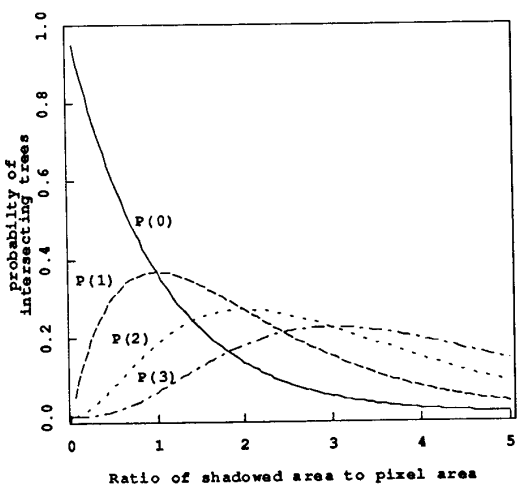


Fig. 3. Probabilities of intersecting trees: $P(n)$ is the probability of intersecting $n$ trees. The horizontal axis represents the ratio of the total area shadowed by trees to the area of ground containing these trees.

without any attenuations from other trees. The $n$ has to be greater than zero in order to have this scattering. When $n = 2$, which means that there is one tree between the radar and scatterer, the corresponding extinction was added.

### B. Ground-Crown Interaction Term

$$\begin{aligned} \boldsymbol{M}^0_{t-s} &= \boldsymbol{M}^0_{s-c} + \boldsymbol{M}^0_{c-s} + \boldsymbol{M}^0_{scs} \\ &= \sum_{n=0}^{\infty}\sum_{m=1}^{\infty}[P(m)e^{-\kappa_c^+(m-1)\bar{s}}\boldsymbol{M}_{s-c}e^{-\kappa_c^-n\bar{s}}P(n)] \\ &\quad + \sum_{n=1}^{\infty}\sum_{m=0}^{in}[P(m)e^{-\kappa_c^+m\bar{s}}\boldsymbol{M}_{c-s}e^{-\kappa_c^-(n-1)\bar{s}}P(n)] \\ &\quad + \sum_{n=1}^{n=\infty}[P(n)e^{-\kappa_c^+(n-1)\bar{s}}\boldsymbol{M}_{scs}e^{-\kappa_c^-(n-1)\bar{s}}]. \end{aligned} \tag{19}$$

### C. Backscattering from the Ground Surface

$$\begin{aligned} \boldsymbol{M}^0_s &= \boldsymbol{M}^0_{s1} + \boldsymbol{M}^0_{s2} \\ &= \sum_{n=0}^{\infty}[P(n)e^{-\kappa_c^+n\bar{s}}\boldsymbol{M}_s e^{-\kappa_c^-n\bar{s}}]. \end{aligned} \tag{20}$$

### D. Ground-Trunk Interaction Term

$$\boldsymbol{M}^0_{t-s} = \sum_{n=0}^{\infty}[P(n)e^{-\kappa_c^+n\bar{s}}\boldsymbol{M}_{t-s}e^{-\kappa_c^-n\bar{s}}] \tag{21}$$

and the total backscattering Stokes matrix will be:

$$\boldsymbol{M}^0 = \boldsymbol{M}^0_t + \boldsymbol{M}^0_{t-s} + \boldsymbol{M}^0_s + \boldsymbol{M}^0_{t-s}. \tag{22}$$

The Stokes matrix calculated above fully characterizes the backscattering of targets. By wave synthesis, the total powers received in any transmit and receiving configuration can be derived from the Stokes matrix. If only the backscattering coefficients in *HH*, *HV*, *VV*, and *VH* are required, the following are the conversion equations:

$$\begin{aligned} \sigma^0_{vv} &= 4\pi\boldsymbol{M}_{1,1}; \quad \sigma^0_{vh} = 4\pi\boldsymbol{M}_{1,2} \\ \sigma^0_{hv} &= 4\pi\boldsymbol{M}_{2,1}; \quad \sigma^0_{hh} = 4\pi\boldsymbol{M}_{2,2}. \end{aligned} \tag{23}$$

## V. Model Implementation and Simulations

### A. Model Inputs and Simulation Procedure

The input parameters to the model include the average number of trees per pixel ($n$), the average height of trees in a stand ($h$) and standard deviation of tree height ($h_t$); the size and orientation distributions ($p_1(\alpha, \beta)$, ($p_2(h, a)$) and dielectric constants ($\epsilon_n$, $\epsilon_b$, $\epsilon_t$) for needles, branches, and trunks; the dielectric constant ($\epsilon_s$) and roughness ($\sigma$, $l$) of the ground surface; and the radar incidence angle ($\theta$) and wavelength ($\lambda$). In addition, the regression relations between (i) the DBH (Diameter at Breast Height) and total height of trees; and (ii) the DBH and tree-crown-shape parameters $H$ and $R$ derived from field measurements were used to determine the gap probabilities.

### B. Comments on Some Input Parameters for Simulation

*1) Numbers of Needles and Branches per Cubic Meter within Tree Crown:* No direct measurement has been performed nor are such data to be found in the literature at this time. For the Ponderosa pines in Oregon, Gholz *et al.* [14] provided regression equations for calculating the biomasses of the total foliage and live branch from the DBH of the tree. The biomass can be converted to volume if the specific weight is known. From our field measurements, regression relationships for calculating crown length and width from DBH have been derived [12]. Therefore the volume fractions of foliage and branch within a tree crown can be estimated from its DBH or height. The volume fractions can be further converted to the numbers of needles and branches if the dimensions of needle and branch are known. We have used 4000 needles and 10 branches per cubic meter of crown for simulations performed in this chapter.

*2) Orientation Distributions of Needles, Branches and Trunks:* For the Ponderosa pine in the simulations performed in this section, the branches are assumed to have an average size of 0.75-m long and 0.04-m in diameter, with uniform distributions within the range of $\pm 40\%$ of the mean values. The needles are 0.10-m long and 0.001-m in diameter and assumed to be uniformly distributed in both the azimuth and zenith directions. From the field observations, the branches of Ponderosa pines appear to be preferably horizontally oriented. Because there is no field measurement of this orientation, the branches are assumed to be a uniform distribution in the azimuth direction and a probability density function in the zenith ($\alpha$) direction described by:

$$p(\alpha) = \begin{cases} \sin^2\alpha \Big/ \int_0^{\pi}\sin^2 x\,dx, & \text{if } 0 \le \alpha \le \pi \\ 0, & \text{otherwise.} \end{cases} \tag{24}$$

Trunks are assumed to be vertical in all the sensitivity simulations, while in the simulations of backscattering coefficients for eight forest stands, trunk orientations are assumed to be uniform in the azimuth direction and have a specified distribution in the zenith direction (Fig. 9).

*3) Dielectric Constants of Trunk, Branches, and Needles:* Dielectric constants were measured using dielectric probes. Field dielectric measurements are not very stable because they depend on several factors, such as the stability of instrument, the contact surface between the probe and material, and the pressure when the probe is pushed to the surface, etc. The data may only give us rough estimates of the dielectric constants. The dielectric constants of branches are lower than those for trunks based on our field measurements [15]. Only a few measurements of the branch dielectric constant were conducted due to the difficulties of measurement and time constraints. There were too few data to make a reasonable selection. Measurements of dielectric constants of needles are extraordinarily difficult by this method due to the lack of a contact surface, extreme sensitivity to pressure, and angular variation in placement. Therefore in our simulations the dielectric constants were assumed to be the same for trunk, branch, and needles. The data we chose for simulations for the $C$, $L$, and $P$ bands are $22.5-i7.5$; $20.0-i50$; and $20.0-i4.0$, respectively.

*4) Surface Roughness and Dielectric Constant:* In our simulations for comparing the results from three different bands ($C$, $L$, and $P$), we assumed a very smooth surface with a standard deviation of height 0.003 m and correlation length 0.03 m in order to use the small perturbation model for all three bands so that the simulated results could be compared. For simulations performed at $L$ and $P$ bands for forest stands at Mount Shasta, surface roughness is adjusted to have a standard deviation of height 0.01 m and correlation length 0.1 m. The dielectric constant of the surface is assumed to be $7.0-i1.5$, the same as that we used earlier [1].

## VI. Simulation Results

The following are some simulation results and graphs using the model developed in this section. When the backscattering coefficients at *HH*, *VV*, and *HV* polarizations are plotted (e.g., Fig. 7), the total backscattering, crown backscattering, trunk–ground backscattering, direct backscattering from ground surface, and crown–ground backscattering components are designed by 1, 2, 3, 4, and 5 at each point on the curves, respectively. For plots showing the total backscattering coefficients, *HH*, *VV*, and *HV* polarizations are indicated by 1, 2, and 3, respectively (Fig. 8).

### A. Model Sensitivity Analysis

*1) Backscattering Versus Incidence Angle:* Fig. 4 is a plot of the total backscattering coefficient versus incidence angle at $L$-band, and Fig. 5 shows four backscattering components at different incidence angles. The following can be noticed from these plots:

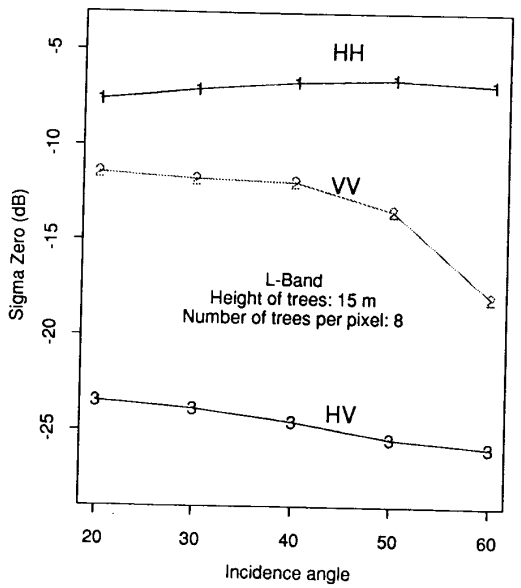


Fig. 4. Backscattering coefficient versus incidence angle: $L$-band, the average number of trees per pixel is 8, and the height is 15 m.

(a) At lower incidence angles (e.g., 20°), trunk–ground, crown–ground, and direct ground backscattering terms at *HH* polarization are comparable. When the incidence angle increases, the trunk–ground term becomes dominant due to the drop of the crown-ground and direct ground backscattering terms. Hence, *HH* polarization are largely determined by the trunk–ground-scattering mechanism. For *VV* polarization, at low incidence angle the trunk–ground term is comparable to the crown–ground and direct surface-backscattering terms, while at high incidence angle it is comparable to the crown backscattering. The trunk–ground term is the dominant term in the range of about 30°–50° at *VV* polarization.

It is expected that the crown-volume backscattering will increase when the incidence angle increases in the case of the discontinuous forest stands. The crown–ground double-bounce backscattering decreases with the increase of incidence angles.

(b) Crown backscattering increases at all polarizations with the increase of incidence angle, but has only a minor contribution to the total backscattering. At the shorter wavelengths and for a closed canopy, crown backscattering may become dominant (see the simulation results in Tables III, V, and VI at $C$-band), so the changing pattern of backscattering with incidence angles will basically be similar to the volume backscattering.

(c) The cross-polarization term (*HV*) is determined by the crown and crown–ground backscattering.

*2) Backscattering Versus Number of Branches per Cubic Meter Within the Tree Crown:* In Fig. 6 the number

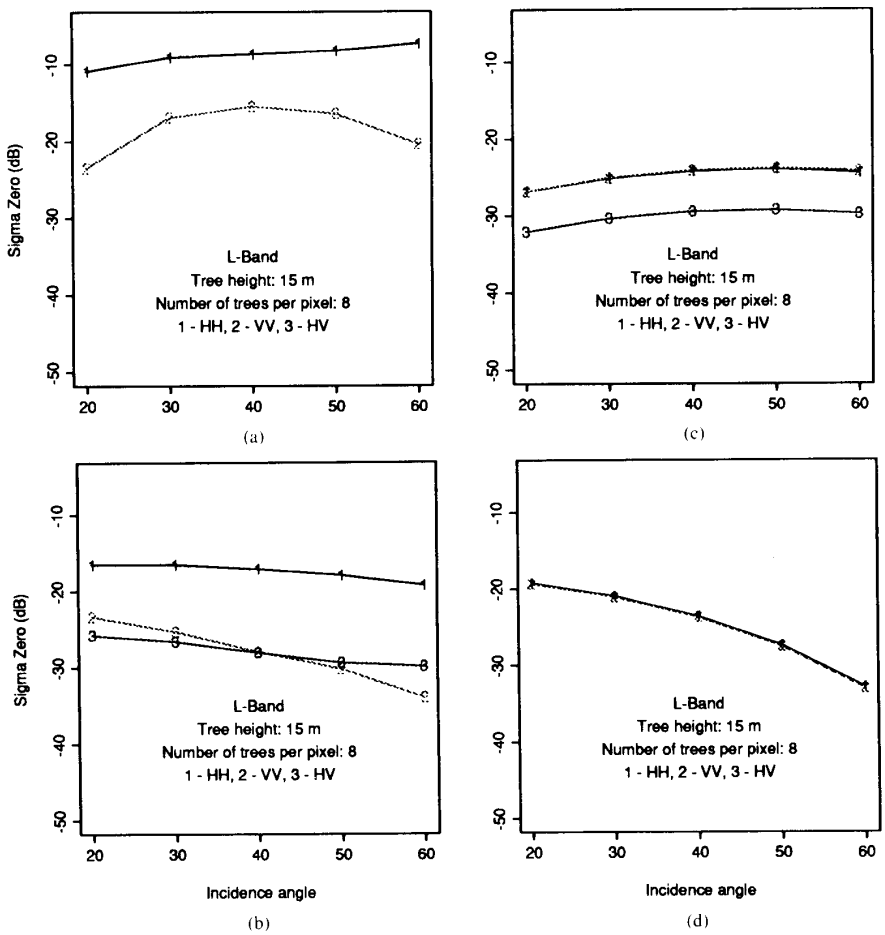


Fig. 5. Backscattering coefficients of four components versus incidence angle: *L*-band, the average number of trees per pixel is 8, and the height is 15 m. (a) Trunk-ground backscattering. (b) Crown-ground backscattering. (c) Crown back scattering. (d) Direct ground backscattering.

of branches (along with the number of needles) changes (see figure caption). The crown and crown-ground backscattering terms increase with the increase of branches and needles, while the trunk–ground and direct surface-backscattering drops slightly due to the increased extinction. The change of the total backscattering coefficients at *HH* is very small here. The cross-polarization term (*HV*) increases, since it is determined by crown and crown-ground scatterings. The cross-polarization signature may therefore have more power than the co-polarization signature in discriminating between forests of different species.

*3) Backscattering Versus Number of Trees Per Pixel:* Fig. 7 shows the backscattering coefficients at *L*-band in relation to the number of trees per pixel. Obviously, the backscattering coefficients at all three polarizations and of all components except the direct ground-surface term increase with the increase of the number of trees per pixel.

*4) Backscattering Versus Tree Height:* Fig. 8 shows that backscattering increases with the increase in tree height. The ripples in *HH* and *VV* plots are from the trunk-ground term, since the scattering amplitude from a dielectric cylinder is heavily influenced by a *sin* term, and this term is quite sensitive to the length of the cylinder.

### *B. Backscattering Coefficients of Eight Forest Stands in Mount Shasta Forest*

The eight forest stands were modeled in [5] by Sun and Simonett using a continuous canopy model. Trees at these forest stands have relatively small crowns, many of which are short and atop the trees. While some stands may be too open to be considered to have a close canopy, some are certainly too close to use the model proposed here (Table I). Nevertheless, the backscattering coefficients of the eight forest stands are simulated using the model and compared with the NASA/JPL Aircraft SAR data in Tables II–IV. Trunks with a leaning angle (departure from vertical) randomly chosen from the distribution shown in Fig. 9 were used in the simulation. A total of 100 pixels

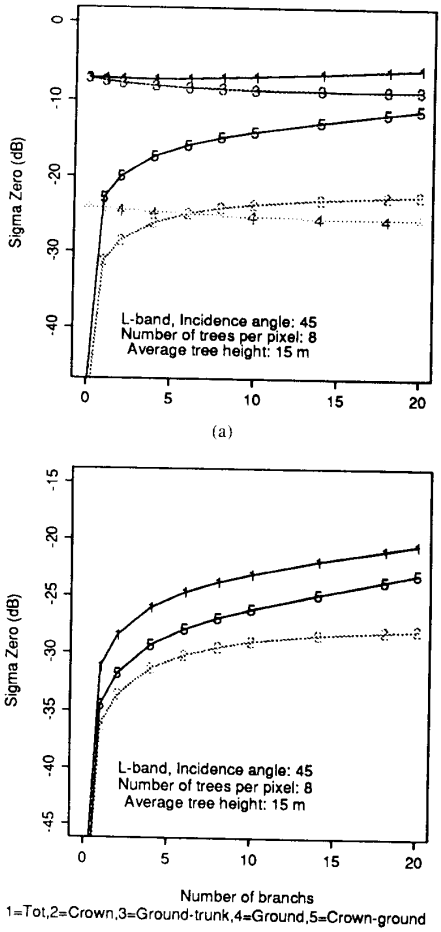


Fig. 6. Backscattering coefficients versus number of branches per cubic meter within tree crown: $L$-band, 45°, average branch size—0.75-m long with a radius of 0.02 m. The number of branches change from 0 to 20, while the number of needles changes from 0 to 8000 per cubic meters within the tree crown. (a) $HH$ backscattering coefficient. (b) $HV$ backscattering coefficient.

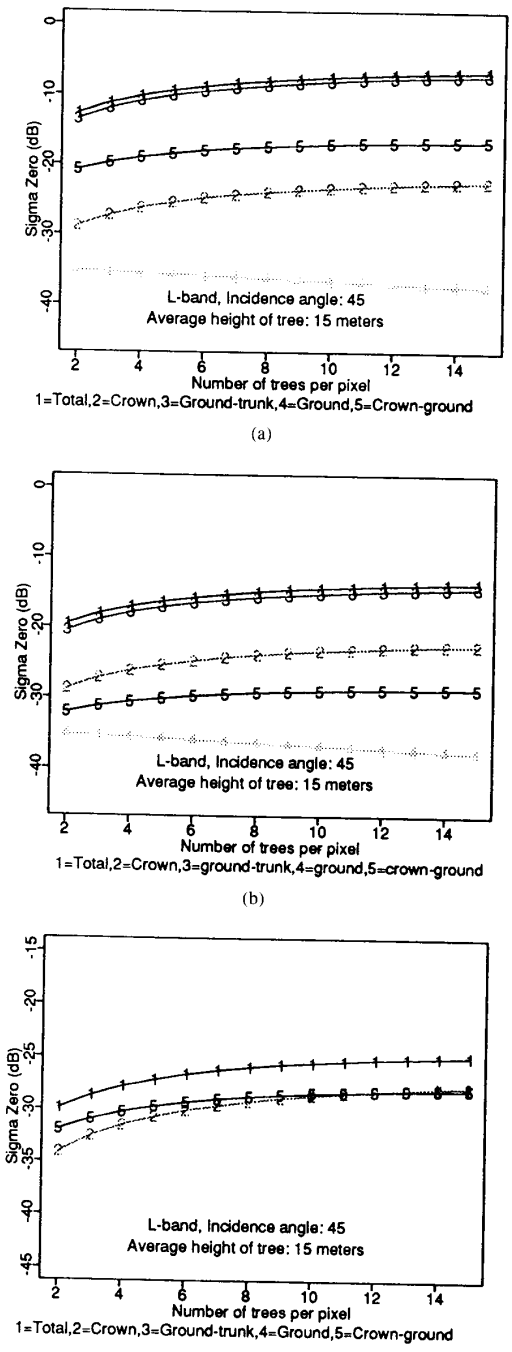


Fig. 7. Backscattering coefficient versus number of trees: $L$-band, the incidence angle is 45°, and the average tree height is 15 m. (a) $HH$ backscattering. (b) $VV$ backscattering. (c) $HV$ backscattering.

are simulated for each forest stand, and then the mean backscattering coefficient is calculated.

The SAR image, which was flown on September 6, 1989 and calibrated by use of corner reflectors, covers only five forest stands. Two Ponderosa plantations (stands 7 and 8) have been missed and the trees at stand 6 have been cut off before this flight.

Tables II and III are the backscattering coefficients of these forest stands from SAR image and model simulations. The differences between SAR data and simulation results in Table IV show that the model prediction at $L$- and $P$-bands are within the standard deviation of SAR data, while at $C$-band, however, the simulated backscattering coefficients are much higher than the SAR data. From Tables V and VI, it can be seen that the dominant backscattering term at $C$-band is the direct backscattering from the tree crown instead of the trunk-ground term as at $L$- and $P$-bands. The possible improper input tree parameters (number of needles and branches and their dielectric constants) to this simulation, which influence backscattering significantly at $C$-band but not at $L$- and $P$-bands, may have caused this problem.

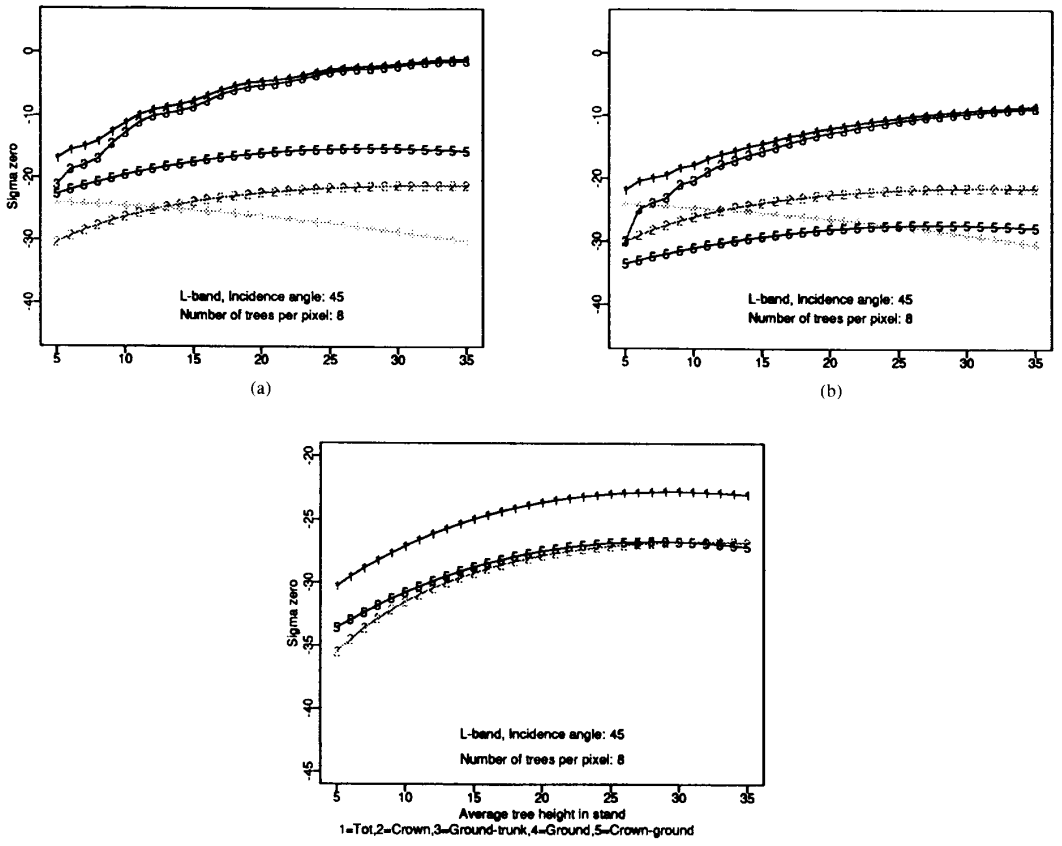


Fig. 8. Backscattering coefficient versus tree height: *L*-band, the incidence angle is 45°, and the number of trees per pixel is 8. (a) *HH* backscattering coefficient. (b) *VV* backscattering coefficient. (c) *HV* backscattering coefficient.

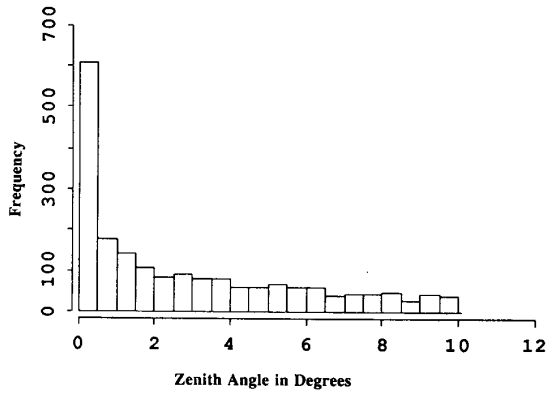


Fig. 9. Distribution of trunk zenith angle used for simulation of backscattering coefficients from forest stands at Mount Shasta Forests, California.

TABLE I
STATISTICS OF THE EIGHT FOREST STANDS

| Stand | 1 | 2 | 3 | 4 | 5 | 6 | 7 | 8 |
|---|---|---|---|---|---|---|---|---|
| $n$ | 26 | 19 | 22 | 48 | 29 | 23 | 38 | 52 |
| $h$ | 20.7 | 24.2 | 16.4 | 24.4 | 18.1 | 18.2 | 13.6 | 12.3 |
| $h_r$ | 11.8 | 9.2 | 5.7 | 9.6 | 7.8 | 11.9 | 2.5 | 2.0 |

$n$—Average tree number in a radar resolution pixel (25 × 25 m). $h$—Average tree height of the stand in meters. $h_r$—Standard deviation of tree height in the stand.

Table VII gives the differences of simulation results at *L*-band between two cases: Vertical trunks and trunks with a leaning angle. It shows that when the trunk is assumed to be vertical to the ground, the differences between *HH* and *VV* backscattering are large and the cross polarization return is very low. A leaning angle for each trunk modifies the simulation results, so that the simulation results become reasonably good compared to the SAR measurements.

## VII. Concluding Remarks

1) From the sensitivity analysis and simulation of backscattering coefficients of forest stands, the model appears to give a reasonable prediction of backscattering

TABLE II
BACKSCATTERING COEFFICIENTS FROM JPL SAR IMAGES OF FOREST STANDS AT MOUNT SHASTA, CALIFORNIA. THE SD IS THE STANDARD DEVIATION OF AN AREA OF 10 BY 10 PIXELS

| Stand ($\theta$) | | *P*-Band | | | *L*-Band | | | *C*-Band | | |
|---|---|---|---|---|---|---|---|---|---|---|
| | | *HH* | *VV* | *HV* | *HH* | *VV* | *HV* | *HH* | *VV* | *HV* |
| Stand 1 (37.1°) | mean | −6.22 | −8.31 | −13.04 | −6.69 | −7.40 | −12.02 | −7.23 | −6.75 | −12.28 |
| | SD | 2.68 | 3.22 | 2.37 | 2.36 | 2.79 | 2.67 | 3.17 | 2.69 | 3.39 |
| Stand 2 (40.5°) | mean | −6.71 | −8.63 | −14.11 | −6.50 | −7.98 | −11.95 | −9.98 | −10.00 | −15.24 |
| | SD | 3.48 | 2.91 | 2.64 | 2.79 | 2.91 | 2.49 | 2.94 | 2.83 | 3.18 |
| Stand 3 (43.5°) | Mean | −8.38 | −11.19 | −15.9 | −8.18 | −10.47 | −14.91 | −9.79 | −10.65 | −15.42 |
| | SD | 3.05 | 3.33 | 3.81 | 2.99 | 3.66 | 3.42 | 3.47 | 3.52 | 3.71 |
| Stand 4 (41.0°) | Mean | −6.31 | −8.70 | −13.30 | −6.99 | −8.51 | −12.34 | −8.32 | −8.41 | −14.36 |
| | SD | 2.61 | 3.02 | 3.13 | 2.94 | 2.88 | 3.00 | 4.24 | 4.38 | 3.15 |
| Stand 5 (44.5°) | mean | −7.20 | −8.99 | −13.39 | −7.67 | −9.40 | −12.56 | −11.75 | −11.09 | −16.93 |
| | SD | 3.16 | 2.83 | 2.97 | 2.85 | 2.95 | 3.28 | 3.15 | 3.37 | 3.42 |

TABLE III
SIMULATION RESULTS: TOTAL BACKSCATTERING

| Stand | *P*-Band | | | *L*-Band | | | *C*-Band | | |
|---|---|---|---|---|---|---|---|---|---|
| | *HH* | *VV* | *HV* | *HH* | *VV* | *HV* | *HH* | *VV* | *HV* |
| Stand 1 | −6.81 | −8.76 | −12.45 | −5.21 | −8.36 | −11.23 | −1.42 | −1.13 | −7.92 |
| Stand 2 | −7.91 | −10.56 | −14.11 | −4.40 | −7.33 | −10.50 | −1.80 | −1.51 | −8.29 |
| Stand 3 | −10.44 | −13.45 | −16.83 | −6.35 | −9.03 | −12.56 | −2.56 | −2.26 | −9.04 |
| Stand 4 | −6.20 | −7.88 | −11.70 | −5.81 | −9.48 | −12.13 | −1.32 | −1.03 | −7.82 |
| Stand 5 | −8.48 | −11.20 | −14.44 | −5.13 | −8.08 | −11.17 | −1.95 | −1.66 | −8.44 |
| Stand 6 | −8.29 | −11.17 | −14.22 | −4.53 | −7.38 | −10.26 | −2.42 | −2.12 | −8.90 |
| Stand 7 | −10.12 | −13.02 | −16.28 | −7.06 | −9.79 | −13.11 | −2.07 | −1.77 | −8.55 |
| Stand 8 | −9.86 | −12.71 | −16.12 | −7.27 | −10.07 | −13.46 | −1.85 | −1.53 | −8.32 |

TABLE IV
DIFFERENCES (SAR DATA MINUS SIMULATED TOTAL BACKSCATTERING)

| Stand | *P*-Band | | | *L*-Band | | | *C*-Band | | |
|---|---|---|---|---|---|---|---|---|---|
| | *HH* | *VV* | *HV* | *HH* | *VV* | *HV* | *HH* | *VV* | *HV* |
| Stand 1 | 0.59 | 0.45 | −0.59 | −1.48 | 0.96 | −0.79 | −5.81 | −5.62 | −4.36 |
| Stand 2 | 1.20 | 1.93 | 0.00 | −2.10 | −0.65 | −1.45 | −8.18 | −8.49 | −6.95 |
| Stand 3 | 2.06 | 2.26 | 0.93 | −1.83 | −1.44 | −2.34 | −7.23 | −8.39 | −6.38 |
| Stand 4 | −0.11 | −0.82 | −1.60 | −1.18 | 0.97 | −0.21 | −7.00 | −7.38 | −6.54 |
| Stand 5 | 1.28 | 2.21 | 1.05 | −2.54 | −1.32 | −1.39 | −9.80 | −9.43 | −8.49 |

TABLE V
SIMULATION RESULTS: TRUNK–GROUND BACKSCATTERING

| Stand | *P*-Band | | | *L*-Band | | | *C*-Band | | |
|---|---|---|---|---|---|---|---|---|---|
| | *HH* | *VV* | *HV* | *HH* | *VV* | *HV* | *HH* | *VV* | *HV* |
| Stand 1 | −6.90 | −8.87 | −12.54 | −5.72 | −9.29 | −11.75 | −46.63 | −51.61 | −53.57 |
| Stand 2 | −8.01 | −10.66 | −14.19 | −4.92 | −8.11 | −10.93 | −44.66 | −49.58 | −54.59 |
| Stand 3 | −10.54 | −13.56 | −16.92 | −7.20 | −10.31 | −13.18 | −48.42 | −53.49 | −57.04 |
| Stand 4 | −6.29 | −7.97 | −11.78 | −6.35 | −10.68 | −12.79 | −52.39 | −58.69 | −61.35 |
| Stand 5 | −8.58 | −11.30 | −14.53 | −5.72 | −9.00 | −11.66 | −47.39 | −52.52 | −54.94 |
| Stand 6 | −8.39 | −11.28 | −14.30 | −5.07 | −8.19 | −10.63 | −46.15 | −51.22 | −53.87 |
| Stand 7 | −10.23 | −13.13 | −16.37 | −7.99 | −11.24 | −13.85 | −49.69 | −55.04 | −58.10 |
| Stand 8 | −9.97 | −12.82 | −16.21 | −8.20 | −11.55 | −14.29 | −50.90 | −56.56 | −59.11 |

TABLE VI
SIMULATION RESULTS: DIRECT CROWN BACKSCATTERING

| Stand | *P*-Band | | | *L*-Band | | | *C*-Band | | |
|---|---|---|---|---|---|---|---|---|---|
| | *HH* | *VV* | *HV* | *HH* | *VV* | *HV* | *HH* | *VV* | *HV* |
| Stand 1 | −33.10 | −32.58 | −44.95 | −15.68 | −15.92 | −20.90 | −1.42 | −1.13 | −7.92 |
| Stand 2 | −33.91 | −33.46 | −45.79 | −16.26 | −16.49 | −21.48 | −1.80 | −1.51 | −8.29 |
| Stand 3 | −35.25 | −35.02 | −47.22 | −17.17 | −17.35 | −22.36 | −2.56 | −2.26 | −9.05 |
| Stand 4 | −32.94 | −32.49 | −44.82 | −15.51 | −15.74 | −20.73 | −1.32 | −1.03 | −7.82 |
| Stand 5 | −34.24 | −33.95 | −46.18 | −16.34 | −16.55 | −21.55 | −1.95 | −1.66 | −8.44 |
| Stand 6 | −34.81 | −34.53 | −46.76 | −16.83 | −17.03 | −22.03 | −2.42 | −2.12 | −8.90 |
| Stand 7 | −34.81 | −34.67 | −46.83 | −16.65 | −16.81 | −21.83 | −2.08 | −1.77 | −8.55 |
| Stand 8 | −34.63 | −34.53 | −46.67 | −16.43 | −16.57 | −21.60 | −1.85 | −1.53 | −8.32 |

TABLE VII
COMPARISONS OF SIMULATION RESULTS AT *L*-BAND FROM TWO CASES: VERTICAL TREE TRUNKS (SIMU 1) AND A RANDOM LEANING ANGLE WAS ASSIGNED TO EACH TRUNK (SIMU 2)

| Stand | 1 | | | 2 | | | 3 | | | 4 | | | 5 | | |
|---|---|---|---|---|---|---|---|---|---|---|---|---|---|---|---|
| Pol. | *HH* | *VV* | *HV* | *HH* | *VV* | *HV* | *HH* | *VV* | *HV* | *HH* | *VV* | *HV* | *HH* | *VV* | *HV* |
| SIMU 1 | −4.94 | −11.01 | −20.50 | −4.975 | −10.79 | −20.21 | −5.75 | −10.83 | −20.54 | −3.03 | −9.69 | −20.58 | −4.54 | −10.37 | −20.39 |
| SIMU 2 | −5.21 | −8.36 | −11.23 | −4.40 | −7.33 | −10.50 | −6.35 | −9.03 | −12.56 | −5.81 | −9.48 | −12.13 | −5.13 | −8.08 | −11.17 |

coefficients at multiple wavelengths, multiple incidence angles, and multiple polarizations.

2) The overwhelming dominance of the double-bounce terms at *L*- and *P* bands arises predominantly from the corner reflector effect. This effect was enhanced by two major factors: (a) The smooth surface of the trunk—this raises the specular reflection of the trunk; and (b) idealization of ground surface—many factors have been ignored in simulation such as the slope of the surface near the trunk, dead wood on the ground, understories, etc. Alternative models may be needed for trunk and ground surfaces. If the tree trunks are modeled as cylinders or truncated cones with rough surfaces, the ground surface is rough and the angles between the trunks and ground surface is not equal to 90° due to the leaning of trunks and/or the surface slope, the trunk–ground double-bounce scattering will not necessarily occur in the specular directions. Both trunk and ground surfaces will also scatter incident waves to the directions other than the specular direction and the calculation of radar backscattering will involve an integration over the entire scattering angles at the trunk and ground surfaces.

3) The shape of tree crowns and gap probabilities have been introduced into the radar backscatter model so that the model can be reasonably used for discontinuous stands. The model can also be used for different types of forests by using specific crown shapes. This model, however, doesn't take the gap size distribution or spatial clustering of trees into account, since the trees are assumed to be randomly distributed within a stand. Knowledge about gaps, spatial clustering of trees is very important for understanding forest dynamics and identifying the ecological states of forests. The modeling of radar response to gap distribution and clustering is a challenge to the radar backscatter modeler.

## ACKNOWLEDGMENT

The authors would like to thank the anonymous reviewers for their critics and suggestions.

## REFERENCES

[1] J. A. Richards, G. Q. Sun, and D. S. Simonett, "*L*-band radar backscatter modeling of forest stands," *IEEE Trans. Geosci. Remote Sensing*, vol. GE-25, pp. 487-498, July 1987.

[2] M. A. Karam and A. K. Fung, "Electromagnetic scattering from a layer of finite length, randomly oriented, dielectric, circular cylinders over a rough interface with application to vegetation," *Int. J. Remote Sensing*, vol. 9, no. 6, pp. 1109-1134, 1988.

[3] F. Ulaby, K. Sarabandi, K. McDonald, M. Whitt, and M. Dobson, "Michigan Microwave Canopy Scattering Model (MIMICS)," Univ. Michigan, Ann Arbor, Rep. 022486-T-1, 1988.

[4] S. J. Durden, J. J. van Zyl, and H. A. Zebker, "Modeling and observation of the radar polarization signature of forested areas," *IEEE Trans. Geosci. Remote Sensing*, vol. 26, pp. 290-301, 1988.

[5] G. Q. Sun and D. S. Simonett, "Simulation of *L*-band *HH* radar backscattering for coniferous forest stands: a comparison with SIR-B data," *Int. J. Remote Sensing*, vol. 9, no. 5, pp. 907-925, 1988.

[6] N. S. Chauhan and R. H. Lang, "Microwave modeling of orchard canopy," in *Proc. IGARSS'88*, 1988, pp. 1757-1760.

[7] G. T. Ruck, D. E. Barrick, W. D. Stuart, and C. K. Krichbaum, *Radar Cross Section Handbook*. New York: Plenum, 1970.

[8] C. F. Bohren and D. R. Huffman, *Absorption and Scattering of Light by Small Particles*. New York: Wiley, 1983.

[9] J. J. van Zyl, "On the importance of polarization in radar scattering problems," Ph.D. thesis, California Inst. Technol., Pasadena, 1986.

[10] L. Tsang, J. A. Kong, and R. T. Shin, *Theory of Microwave Remote Sensing*. New York: Wiley-Interscience, 1985, pp. 629-642.

[11] X. Li and A. H. Strahler, "Modeling the gap probability of a discon-

tinuous vegetation canopy," *IEEE Trans. Geosci. Remote Sensing*, vol. 26, pp. 161–170, 1988.
[12] G. Q. Sun, "Radar backscatter modeling of coniferous forest canopies," Ph.D. dissertation, Univ. California, Santa Barbara, 1990.
[13] A. L. Getis and R. Jackson, "The expected proportion of a region polluted by K sources," *Geogr. Anal.*, vol. 3, pp. 256–261, 1971.
[14] H. L. Gholz, C. C. Grier, A. G. Campbell, and A. T. Brown, "Equations for estimating biomass and leaf area of plants in the pacific northwest," Forest Res. Lab., School of Forestry, Oregon State Univ., Corvallis, Res. Paper 41; see also, *IEEE Trans. Geosci. Remote Sensing*, vol. GE-26, pp. 161–170, Mar. 1988.
[15] L. Hess and D. S. Simonett, "Dielectric properties of two western coniferous tree species," in *Proc. IGARSS'90*, 1990, p. 503.

**Guoqing Sun** graduated from the Chinese University of Science and Technology in 1969, majoring in physics. He received the M.S. degree in remote sensing from Nanjing University (China) in 1981, and the Ph.D. degree in geography from the University of California at Santa Barbara in 1990.

His research interests are in image processing, radar backscatter modeling, remote sensing, and Geographic Information Systems. He is currently with Resseler Associates, Inc., Laurel, MD.

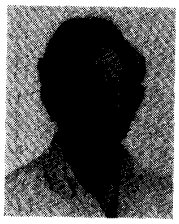

**David S. Simonett** was born in Sydney, Australia. He earned the doctorate degree from the University of Sydney.

He had been a faculty member of the Department of Geography, University of California, Santa Barbara, for the past 16 years, and chaired the Department from 1975 to 1982. He was Co-Director of the David Simonett Center for Spatial Analysis at the time of his death in December 1990, following a long illness. His recent research interests included microwave remote sensing of forests, and geographic information systems. He was a Shuttle Imaging Radar C investigator.

Dr. Simonett was the author of several textbooks and many papers and he received the Distinguished Geographer Award from the Association of American Geographers and the Victoria Medal for Distinguished Accomplishments in Geography from the Royal Geographical Society in England.

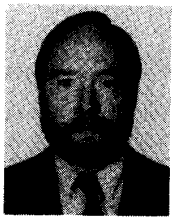

**Alan H. Strahler** (M'86) received the B.A. and Ph.D. degrees in geography from The Johns Hopkins University, Baltimore, MD, in 1964 and 1969, respectively.

He is currently Professor of Geography and Researcher in the Center for Remote Sensing, Boston University, Boston, MA. He has held prior academic positions at Hunter College of the City University of New York, at the University of California, Santa Barbara, and at the University of Virginia. Originally trained as a Biogeographer, he has been actively involved in remote sensing research since 1978. He has been a Principal Investigator on numerous NASA contracts and grants. His primary research interests are in spatial modeling and spatial statistics as they apply to remote sensing, and in geometric-optical modeling of remotely sensed scenes. He is particularly interested in remote sensing of forests and the inference of vegetation canopy parameters from digital images through invertible models.